Effect of Au nanoparticles on the activity of TiO_2 for ethanol upgrading reactions

J. Quesada[a], R. Arreola-Sánchez[a,b], L. Faba[a], E. Díaz[a], V. M. Rentería-Tapia[b], S. Ordóñez[a]

[a.] *Department of Chemical and Environmental Engineering, University of Oviedo. Oviedo 33006, Spain. Email: sordonez@uniovi.es Phone: +34985103437 Fax: +34985103443.*

[b.] *Department of Natural and Exact Sciences, Los Valles University Center, University of Guadalajara, Ameca 46600, Jalisco, Mexico*

Abstract

This article analyses the role of gold nanoparticles supported on TiO_2 for the gas-phase ethanol condensation. Previously, the original P25 surface was modified for increasing the Au-Ti interaction, in order to minimize the thermal deactivation. Catalysts were tested both in absence and presence of hydrogen (523 - 673 K, WHSV = 7.9 h^{-1}; y_{EtOH} = 0.32; y_{H2} = 0-0.1; 0.1 MPa). Parent TiO_2 is mainly selective for dehydration reactions yielding diethyl ether (favoured at low temperatures) and ethylene (favoured at higher temperatures). The presence of Au in the catalyst promotes dehydrogenation pathways, yielding acetaldehyde, as well as condensation products (mainly butanol, with selectivities close to 10%). According to DRIFT spectroscopy results, the strong ethanol adsorption on the TiO_2 surface justifies the low yields and the high relevance of side-reactions produced by inter- or intra- molecular dehydration routes (diethyl ether, and ethylene formation). The gold addition minimizes this adsorption and enhances the main route by a double role: an improvement in the dehydrogenation rate (yielding more acetaldehyde) and an enhancement in the hydrogenation steps.

Keywords

Guerbet reaction; DRIFT spectroscopy; Butanol; Aldol condensation; stability

1. Introduction

Although gold was historically considered as a non-active noble metal in heterogeneous catalysis, it shows interesting properties as catalyst or promoter when it is presented as small nanoparticles [1,2]. Indeed, gold is able to catalyse many different reactions (oxidations, decompositions, hydrodechlorination reactions, etc.) at lower temperatures or with higher selectivity than other metal catalysts [3]. Supported gold materials, also promote selective hydrogenation of olefins, being these studies a turning point for gold application in catalysis [4,5]. Based on these preliminary studies, the hydrogenation of α,β-unsaturated aldehydes using gold nanoparticles supported on TiO_2 and ZrO_2 was also studied, considering acrolein and crotonaldehyde as probe molecules [6,7]. Following this approach, Au supported catalysts could be interesting for other reactions, such as the ethanol-to-butanol valorisation, where hydrogen transfer reactions are relevant steps in the reaction mechanism.

Ethanol is nowadays produced from different biomass resources in large amounts [8-10], promoting de development of different valorisation routes. The ethanol gas-phase condensation is one of the most interesting ones, since it allows obtaining different compounds, such as 1,3-butadiene, 1-butanol, larger alcohols, etc., with interesting properties as biofuels and bioplatform molecules, with main attention focused on the 1-butanol [11-13]. The ethanol condensation to obtain this molecule is accomplished by the Guerbet reaction, using basic materials as catalysts [14]. Despite different mechanisms have been proposed, most of the last studies consider the four-step reaction pathway as the predominant in this complex process [15-17]. This reaction mechanism, summarized in the **Scheme 1**, consists of the ethanol dehydrogenation to acetaldehyde, the acetaldehyde self-aldolization to obtain crotonaldehyde and two hydrogenation steps to obtain crotyl alcohol and 1-butanol (main product). The dehydration of crotyl alcohol would also produce 1,3-butadiene as, also of industrial interest. Main efforts to achieve a good selectivities to these compounds have been

focused on the acid-base surface properties of the catalysts (considering the aldolization step as the key path), proposing hydroxyapatites and magnesia as good materials [15,17-18]. However, results are not very conclusive because main route is also conditioned by other steps that involve hydrogen and water molecules [14].

Parallel studies suggest TiO_2 as an interesting alternative because of its good redox properties that can also be very active in aldol condensations. In such a way, it has been tested in the acetaldehyde aldol-condensation, providing better results than other typical materials used for the Guerbet reaction [19-20]. However, this material has very poor performance in reactions involving dehydrogenation steps [20], so it cannot be directly used in the ethanol gas-phase condensation. This fact suggests that the introduction of a dehydrogenation/hydrogenation active metal on the catalytic surface would improve the products yields by enhancing the acetaldehyde production (reducing the α-hydrogen activation energy of the adsorbed ethanol). Moreover, working under reductive conditions (hydrogen feeding) in the presence of the active metal, last hydrogenations could be also favoured [17,20].

Some authors dealt with this drawback suggesting bifunctional materials by supporting different metals that can enhance the acetaldehyde production (reducing the α-hydrogen activation energy of the adsorbed feeding) [21-22]. The different reaction conditions make difficult the direct comparison among these studies. However, the comparison of FTIR peaks of ethanol adsorption when using TiO_2 or Au/TiO_2 [23], as well as the previous results reported for hydrogenation/dehydrogenation reactions [7,24], suggest that this noble metal can be a good candidate for the ethanol condensation. Deposition-precipitation methods are the most extended procedures to prepare the Au/TiO_2, highlighting the good results (small particles, good dispersion, and high impregnation efficiency) obtained when urea is used as promoting molecule (DPU process) [25,26]. These methodologies do not require any treatment at high

temperature and result into very active materials for reaction at soft temperatures. However, a common disadvantage detected in these studies is the instability and sintering process suffered by the Au particles when reactions are carried out at more severe conditions [26-28]. The subsequent deactivation of these materials is justified by the increase in the atom mobility at the highest temperatures. Due to the low surface area of titania supports (around 50 m^2/g for the P25) these movements produce the collapse of different particles in the same pore, and the sintering process, reaching larger metal particle sizes that are catalytically inactive. This disadvantage could be prevented by modifying the original TiO_2 structure, obtaining a support with higher surface area, or by introducing some irregularities in the surface that promotes a stronger interaction between Pt and TiO_2 surface, limiting the natural movement of gold particles.

This article presents the analysis of the results obtained in the ethanol gas-phase reactions using a catalyst based on gold nanoparticles supported on a commercial P25 material (TiO_2). The original surface was modified by adding titanium isopropoxide in order to introduce a Ti-based monolayer on the crystalline surface, enhancing the irregularities of the original one. This procedure has been previously reported, highlighting the good improvement obtained in terms of thermal stability [29-31]. The effect of reductive conditions and the analysis of the evolution of catalytic surface by Diffuse Reflectance Infrared Fourier Transform (DRIFT) spectroscopy highlight as the main new contributions of this study, explaining the products distribution in terms of adsorbed species and metal-support-molecules interactions.

2. Experimental Methods

2.1 Catalysts preparation

The modified titanium dioxide catalyst was prepared by the homogeneous precipitation method. 3 g of TiO_2 P25 (> 99.5 %, Sigma-Aldrich, BET surface area of 35 - 65 $m^2 \cdot g^{-1}$) were suspended in 20 mL of deionized water and after that, 6 mL of titanium(IV) isopropoxide (97 %, Aldrich) were added dropwise and mixed at 363 K under soft agitation for 8 hours. Isopropoxide acts as an oxide overcoating that avoids the "material gap" and "pressure gap", typical phenomena related to the coexistence of more than one crystalline phase. These phenomena justify that metal particles can experience different relative pressure because of different coordinate states, hindering the metal impregnation [32-33]. The mixture was aged at the aforementioned temperature for 48 hours without stirring. Thereafter, the resulting material was dried at 373 K for 24 hours, and calcined in flowing air for 2 hours (5 $K \cdot min^{-1}$ of temperature ramp) at 773 K to obtain the final modified TiO_2.

Regarding to the 1.5 wt % Au/TiO_2 catalyst, the metallic gold nanoparticles were synthesized by the deposition-precipitation with urea method (DPU) [25]. This method was selected considering the previous comparison among different preparation procedures reported in the literature, considering the higher activity observed when using urea instead of the traditional impregnation and photocatalytic deposition [3]. The modified TiO_2 was dried at 373 K for 12 hours before its use as support for the gold deposition to clean the surface. 0.3 g of the modified TiO_2 were mixed with a mixture of 5.5 mL of an aqueous solution ($4.2 \cdot 10^{-3}$ $mol \cdot L^{-1}$) of the gold precursor ($HAuCl_4 \cdot 3H_2O$, 99.9 %, Aldrich) and 20 mL of a urea aqueous solution (98 %, Aldrich; $4.2 \cdot 10^{-1}$ $mol \cdot L^{-1}$). The suspension was kept under stirring during all the process. The temperature of the suspension was increased to 358 K, kept constant under agitation, and protected from light for 24 hours. The progressive decomposition of urea at that temperature releases OH^- anions, which gradually increase the pH of the medium [34-35]. This method allows a slow precipitation of Au^{3+} cations and avoids a high and local rise of the pH, which would induce precipitation in the solution [34]. After the deposition time, the material

was recovered by centrifugation, washed six times with 50 mL of deionized water, and dried at 358 K.

The resulting material was calcined at 773 K in air flow with 5 $K \cdot min^{-1}$ of heating ramp, keeping the final temperature for 2 hours. According to the literature, a heat treatment of at least 400 ^{o}C is required for the full desorption of water [36], and for ensure the complete decomposition of urea [37]. Despite this treatment is not usual for photochemical purposes or when reaction studied is carried out at soft conditions, it is needed to guarantee a physical and chemical stability of this material under the reaction conditions, preventing any influence of changes in the catalytic surface at the studied reaction temperature.

Despite the instability of the Au_2O_3 at these conditions, the complete reduction to Au^0 is not ensured by heating in airflow [38-39]. In order to reduce all the gold of the material and generate the nanoparticles (activation of the catalyst metal phase), the material was treated in hydrogen flow at 573 K for 2 hours with a temperature ramp of 5 $K \cdot min^{-1}$. This treatment allows obtaining highly crystallite phases, epitaxial growth of gold nanoparticles, formation of faceted particles and the complete gold reduction [40].

The 1.5 wt % Au/SiO_2 catalyst, using fumed silica (Sigma, BET surface area of 200 ± 25 $m^2 \cdot g^{-1}$) as support, was synthesized and activated by the same method and procedure as the previously introduced 1.5 wt % Au/TiO_2 material.

2.2 Catalysts characterisation

The morphologic properties were determined by N_2 physisorption at 77 K in a Micromeritics ASAP 2020 using the Brunauer-Emmett-Teller (BET) method to ascertain the surface area, and the Barret-Joyner-Halenda (BJH) method to calculate the pore volume and diameter. The acidity and basicity of the catalysts were analysed by temperature programmed

desorption (TPD) in a Micromeritics 2900 TPD/TPR. 50 mg of solid were pre-treated in helium flow and saturated with CO_2 or NH_3 to determine the basicity or acidity, respectively. The evolution of CO_2 and NH_3 signals were followed using a Pfeiffer Vacuum Omnistar Prisma mass spectrometer as well as the temperature was increased at 2.5 K·min^{-1} from 298 to 823 K. Signals obtained were quantitatively related to the sites concentration after the corresponding calibration of areas obtained. The strength of these sites is directly related to the desorption temperatures. According to our previous results (correlation between TPD and FTIR analyses), basic sites can be divided into weak (293 – 373 K), medium strength (373 – 473 K) and strong (473 – 573 K) [41]. In the same way, according to Arena and co-workers research, acid sites with a desorption temperature lower than 400 K are related to NH_3 physisorbed on weak sites, whereas 473 – 603 K and 653 – 773 K are related to molecules adsorbed on medium and strong sites [42].

The crystalline phases were determined by X-ray diffraction (XRD) in a Philips PW 1710 diffractometer, using CuK_α radiation (45 kV, 15 mA, λ = 1.54 nm). The diffraction intensity was measured in the 2θ range between 5 and 80° at a scanning rate of 0.2 °·min^{-1}. The weight percentage of the anatase and rutile phases (W_A, and W_R, respectively) of the original TiO_2 (P25) and modified TiO_2 (m-P25) catalysts were calculated using the following expressions:

$$\boldsymbol{W_A = 100 \cdot \frac{1}{1 + 1.26 \cdot \frac{I_R}{I_A}}}$$

$$W_R = 100 - W_A$$

Were I_A and I_R are the intensities of the strongest anatase and rutile reflections, respectively [43]. The mean crystallite size of both anatase (L_A) and rutile (L_R) phases for the two materials were determined by the Scherrer equation.

Scanning transmission electron microscopy (STEM) analyses using the Z-contrast technique (high-angle annular dark-field imaging, HAADF) were performed to determine the

particle size and metal dispersion of the gold particles, using a JEOL JEM-2010F equipment operated at 200 keV. The particle size distribution and the average particle diameter were determined by counting over one hundred of gold particles on different areas of the material sample. The average particle diameter (d_{av}) was calculated using the following equation where n_i is the number of particles of d_i diameter:

$$d_{av} = \frac{\sum n_i \cdot d_i^3}{\sum n_i \cdot d_i^2}$$

This expression was used in order to ponder the effect of having different particles sizes in a more accurate procedure that just using the linear diameter. This equation considers the surface effect and it is the most recommended method to analyse particles in the range of nano and micrometres using instrumental methods such as the laser particle size analyser [44].

The diffuse-reflectance UV-Vis spectra of the gold supported over the modified TiO_2 P25 material were determined with a Perkin Elmer Lambda 650 UV/Vis spectrophotometer. The surface composition as well as the metal loading and the oxidation state of Au nanoparticles was measured by X-ray Photoelectron Spectroscopy (XPS), using a SPECS system equipped with a Hemispherical Phoibos detector operating in a constant pass energy, using Mg-Kα radiation ($h \cdot \upsilon$ = 1253.6 eV).

2.3 Catalytic activity studies

Ethanol conversion tests were carried out from 523 to 673 K (50 K of interval) in a 0.4 cm i.d. U-shaped packed bed reactor located inside a controlled electric furnace. The catalyst sample (150 mg; 250-355 μm) was introduced in the reactor where a thermocouple allows the temperature control. The material was pretreated at 523 K for 1 hour in flowing He before each experiment in order to remove any possible adsorbed compound (mainly water). Ethanol

(absolute, VWR) was injected by a syringe pump in the 0.02 $L \cdot min^{-1}$ (STP) flowing H_2-He mixture (10 vol % H_2), obtaining a 32 vol % of ethanol, with a weight hourly space velocity (WHSV) of 7.9 h^{-1}. These conditions were chosen considering those optimized in a previous work [45]. The outgoing gases were on-line analysed with a gas chromatograph (HP6890 Plus) equipped with a flame ionization detector (FID). A TRB-5MS capillary column (30 m, 0.25 mm) was used as stationary phase. The component identification was performed using commercial standards and confirmed by GC-MS (Shimadzu QP-2010) using the same column and methodology as in the GC-FID. The same set of experiments was also performed under inert conditions (He flow instead of He-H_2 mixture).

Conversions were calculated from the ethanol concentration at the reactor inlet and outlet. Selectivities were calculated as the ratio between the concentration of each compound and the sum of the concentrations of all the identified reaction products (acetaldehyde, acetic acid, butanal, crotonaldehyde, crotyl alcohol, diethyl ether, ethyl acetate, ethylene, methane, 1-butanol, 1-hexanol, 1-octanol, 1,3-butadiene, 2-ethylbutanol, and 2-ethylhexanol) considering the carbon atoms of each component. Carbon balances were checked by comparing the total amount of carbon atoms at the reactor inlet and outlet, considering only the identified products.

DRIFT spectroscopy was carried out in a Thermo Nicolet Nexus FT-IR using the Smart Collector Accessory and a MCT/A detector, recording with a resolution of 4 cm^{-1} and collecting 60 scan/spectrum. Samples (20 mg) were placed inside the catalytic chamber where an internal thermocouple allows controlling the temperature of the sample. Materials were pre-treated at 523 K for 1 h in helium flow. Spectra were recorded in the 4000-650 cm^{-1} wavenumber range, after subtraction of the background (KBr pattern). Signals were converted into Kubelka-Munk units to obtain semi-quantitative results. Spectra were collected at similar temperatures and under Ar-H_2 (10 vol % H_2) flow in order to compare the evolution of both gas

and solid phase. The same set of experiments was also carried out under inert conditions (He flow instead of Ar-H_2 mixture).

3. Results and discussion

3.1 Characterization

The textural and surface chemistry properties of the TiO_2, modified TiO_2, and Au supported over modified TiO_2 catalysts are summarized in **Table 1**. The corresponding CO_2 and NH_3 TPD profiles are included as **Fig. 1**. As expected, if commercial and modified supports are compared, a clear effect related to the incorporation of titanium(IV) cations in the TiO_2 is observed. It causes surface defects (cleavage of the surface Ti-O bonds, and subsequent formation of oxygen vacancies), and increases its specific surface area, pore volume, and pore size. These surface defects also lead to higher concentration of active sites (both acid and basic) because of the lower coordination of the surface atoms. Thus, the hydrolysed active gold-containing precursor is expected to condense with the hydroxyls of the support leading to surface-bond nuclei for the condensation of active soluble species, obtaining a higher metal loading with high dispersion. In good agreement to this, a decrease in the surface of Au-material is observed, but the most relevant effect of this deposition is related to the basicity. The high decrease of the concentration of basic sites in the gold-modified catalysts, mainly the strongest ones, whose concentration is much lower than the commercial P25 catalyst, is directly related to the deposition of the gold particles, on the surface anionic species formed upon proton abstraction. At this point, the disappearance of the characteristic band of the TiO_2-support oxygen vacancies after the deposition of Au nanoparticles has been previously demonstrated by Raman studies [46].

The XRD diffraction patterns for the studied materials are shown in **Fig. 2**. The peaks at 2θ = 25.3, 37.8, 48.1, 53.8, 54.9, and 62.7° indicate the presence of the anatase crystalline phase (JCPDS 21-1272), while the peaks at 2θ = 27.4, and 36.0° correspond to the presence of rutile (JCPDS 21-1276). The intensities of the peaks at 2θ = 25.3 and 27.4° are considered as I_A and I_R, respectively, for determining the anatase and rutile fractions. The results of the weight percentage phases of the $mTiO_2$ (W_A = 79 %, and W_R = 21 %) indicate that the introduction of the titanium(IV) cations on the catalytic surface does not modify the crystalline structure of the initial TiO_2 P25 material (W_A = 78 %, and W_R = 22 %). These values correspond to average values of crystallite sizes of the two phases similar for both materials: L_A = 21.9 and 20.4 nm, L_R = 25.6 and 20.5 nm, for TiO_2 and $mTiO_2$, respectively. According to these values, the modification of the support induces the expected decrease in the average value of TiO_2 crystallites, which can increase the interaction between oxide and metal particles, having a positive effect in their thermal stability. As to the $Au/mTiO_2$ diffraction patterns, although the gold load is low (1.5 wt %), two low-intense peaks at 2θ angles of 38.2 and 44.4° related to gold phase (JCPDS 4-784) were observed. The low resolution of these peaks prevents calculate the crystallite size by this technique.

XPS analyses (spectra included in the supplementary information as **Fig. S1**) demonstrate that the structure of $Au/mTiO_2$ is composed by Ti, O, C and Au elements; no other impurities were found. The atomic weight of Au corresponds to a mass percentage of 1.01 %, a bit lower than the theoretical one. This discrepancy is explained by a partial leaching of Au during the preparation method (several washing cycles involved). This value is considered as stable during all the reaction. Ethanol condensation is studied in gas phase, no possible leaching causes are possible at reaction conditions. In good agreement with the literature, signals related to Au 4f where observed, located at 83.55 eV and 87.58 eV. These signals correspond to the $4f_{7/2}$ and $4f_{5/2}$, respectively, and are consistent with the zero oxidation state of metallic Au [47-48]. These results corroborate the high efficiency of reducing procedure applied. On the other

hand, the study of individual analyses focused on the O1s region clearly indicate the presence of one peak around 526 – 529 eV. This peak is directly related to lattice oxygen in anatase TiO_2 [49]. The absence of any other oxygen peak at higher binding energies discards the presence of H_2O, Ti-OH or CO_3^{2-} molecules adsorbed on the catalytic surface that could suggest an incomplete calcination method [50]. On the other hand, the evolution of binding energies of identified O1s peak is in good agreement with the desorption temperatures observed by CO_2-TPD. Thus, these results support the decrease in the general strength of basic sites produced by the modification of TiO_2 surface and the partial recovery of this strength by incorporating the metal phase.

Fig. 3a shows a representative STEM-HAADF image and the histogram of particle size distribution of the Au/mTiO_2 catalyst. A Gaussian distribution, mainly composed of approximately 1.5 and 5 nm size particles, has been observed. These values are congruent with results reported by other authors for similar catalysts [3,47] and correspond to the maximum activity in the ethanol gas-phase condensation observed for gold catalysts prepared using other supports [48]. Therefore, gold nanoparticle sizes of the catalysts used in this work are considered as the optimal for improving the dehydrogenation steps, mainly ethanol to acetaldehyde reaction.

The interaction of light with the metal nanoparticles produces a collective oscillation of the conduction electrons at the interface between the metal and the dielectric medium, creating an electric dipole. This phenomenon is known as "surface plasmon resonance" (SPR) effect, and it is characteristic of gold in the metallic state [49]. The spectrum of the Au/mTiO_2 catalyst (**Fig. 4**) shows two absorption bands, one of them below 400 nm and another between 480 and 700 nm. The former is related to the support absorption [50], whereas the latter is associated with the SPR absorption of the metallic gold nanoparticles (vibration of the conduction electrons) [49]. Concerning this last one band, two contributions of different

position (560 and 608 nm) and intensity can be observed by deconvolution. The differences between the intensity and the position of each band is related to differences in the size of the nanoparticles [18], since there are mainly particles of 5 nm. According to these results, the Au particles are completely reduced, with only evidences of Au^0.

In order to determine the role of the gold nanoparticles in the ethanol condensation reaction, a silica-supported gold catalyst was prepared. As this support is chemically inert (without surface basic and acid sites observed by TPD analyses), only catalytic effect associated to the metal will be observed. Because of this reason, as this material is only used as a "blank" test for the metal role, only analyses focused on the metal size crystalline were done. This catalyst was also analysed by STEM-HAADF imaging. **Fig. 3b** shows a representative micrograph of the catalyst and the particle size histogram. Even though the gold particles were slightly smaller than those previously observed in the case of the $Au/mTiO_2$ catalyst, the particle mean size (5.0 nm) were quite similar, enabling the direct comparison of both gold-containing catalysts without taking into account structure-sensitivity aspects. XPS analysis of this material is shown in **Fig. S2**. No relevant signals associated to Au $4f_{5/2}$ nor $4f_{7/2}$ were detected with enough resolution, being not possible the determination of the actual metal loading. This result is explained by the low amount of Au expected and the proximity of main signals related to Si2p that can disrupt the general spectrum. The plasmon band was also analysed for this material, being the spectrum added to the supplementary information (**Fig. S3**), in order to compare it with the SPR of $Au/mTiO_2$. In general terms, main differences between both materials are related to the signal position (with a maximum at 522 nm for the SiO_2 support) as well as the lower intensity observed for this silica. These differences are justified by the higher dielectric constant of the surrounding medium of $mTiO_2$. The deconvolution of this spectrum is congruent with the particle mean size previously determined (5 nm).

3.2 Catalytic activity

The evolution of the conversion and carbon balance closure working under reductive conditions for the TiO_2, $mTiO_2$, and $Au/mTiO_2$ catalysts are shown in **Fig. 5**. At working conditions and considering the small size of both, reactant and products, the mass transfer effects can be discarded, being the experimental results directly related to the catalytic activity of each material. This hypothesis was previously checked in same reaction at similar conditions [45]. Both the conversion and the carbon balance follow the same trends for the three considered materials (increasing conversions at increasing temperatures; decreasing carbon balances). Conversions follow the order $TiO_2 < mTiO_2 < Au/TiO_2$, being the differences more important as temperature increases, reaching a difference of 20 % between the conversion with the Au/TiO_2 and the unsupported material. These results involve an improvement because of the metal but also an improvement because of the modification of the original surface, introducing the irregularities needed to maximize the active sites available. Thus, the conversion obtained with Au/TiO_2 at 673 K (74.2 %) is, to the best of our knowledge, among the highest conversions reported for this reaction at these reaction conditions [51-53]. In order to corroborate the absence of diffusional limitations, these results (the worst scenery) were used to determine the Thiele modulus (obtaining a value of 0.09 that corresponds to a $\eta\phi^2$ of $5.18 \cdot 10^{-2}$) and the Carberry value (with a result of $1.15 \cdot 10^{-6}$). According to these values, both diffusional limitations are far from the threshold values leading to relevant effects of mass transfer on the overall kinetics. If conversions are normalized by basic sites (the active sites for this reaction in the cases of the non-metallic catalysts), activity of the $Au/mTiO_2$ at 523 K is 3.6 and 4.5 times higher than the corresponding to TiO_2 and $mTiO_2$ catalysts, respectively. This suggests a relevant role of gold and reducing conditions in the final conversion, since the $Au/mTiO_2$ catalyst has a lower concentration of active sites and specific surface area (**Table 1**).

The highest carbon balances closures were observed for the TiO_2 at all the studied temperatures, whereas no relevant differences were observed between values obtained for $mTiO_2$ and $Au/mTiO_2$, except at the highest temperature studied. At these conditions, the balance closure is significantly lower with the metallic catalyst (68.1 %, $Au/mTiO_2$ at 673 K).

The selectivities to the different reaction products obtained with the studied catalysts are also shown in **Fig. 5**. Acetaldehyde selectivities are considerably higher with the $Au/mTiO_2$ at 523 K (TiO_2: 37.7 %; $mTiO_2$: 45.9 %; $Au/mTiO_2$: 68.5 %) and 573 K (TiO_2: 16.4 %; $mTiO_2$: 15.6 %; $Au/mTiO_2$: 57.6 %). Although at the highest temperatures acetaldehyde selectivity is lower for the $Au/mTiO_2$ than for $mTiO_2$, the sum of the selectivities to acetaldehyde and all of the long chain chemicals produced from acetaldehyde (crotonaldehyde, crotyl alcohol, 1-butanol, butanal and ethyl acetate) are always the highest (TiO_2: 19.3 and 29.9 %, $mTiO_2$: 25.1 and 36.9 %, $Au/mTiO_2$: 34.2 and 38.0 %, at 623 and 673 K respectively). This fact corroborates the promoting effect of the metal on the ethanol dehydrogenation step, especially at low temperatures. However, at higher temperatures the values of acetaldehyde selectivities are more similar among the three different materials, because subsequent condensation steps take place at larger extent. This fact suggests that the alcohol dehydrogenation becomes less relevant as temperature increases, comparing to other competitive reactions (dehydration to diethyl ether, and mainly to ethylene), masking the effect of the metal on the dehydrogenation reactions.

Highest selectivities to diethyl ether (side product) were observed for TiO_2 and $mTiO_2$ catalysts, leading to a decrease of acetaldehyde formation (main route). This effect is more remarkable at lowest temperatures (72.9 and 71.2 % diethyl ether selectivity at 573 K with the TiO_2 and $mTiO_2$, respectively). These values are also higher than those reported in the literature for other catalysts tested in this reaction (hydroxyapatites, Mg-Al mixed oxides, MgO) [54-56]. Therefore, a strong interaction between ethanol and the surface with these materials is suggested, as diethyl ether is produced from two ethanol molecules by reaction

coupling followed by a dehydration. This is in agreement with the strongest interaction between ethanol and titania, comparing with other materials (magnesia and hydroxyapatites) previously reported by Young and coworkers [20]. In the case of the Au/mTiO_2 material, the presence of the active metal phase on the catalytic surface, which promotes the ethanol dehydrogenation, leads to lower diethyl ether selectivity at low temperatures (94 % lower than the mTiO_2-support at 523 K). However, the diethyl ether selectivity at the highest temperatures - especially at 673 K - are similar comparing the three catalysts (27.3, 23.0, and 26.5 % with the TiO_2, mTiO_2, and Au/mTiO_2, respectively), which is in agreement with the faster reaction rates of dehydration steps at the highest temperature. Likewise, ethylene selectivities increase with the temperature for the three catalysts, being lower with the Au/mTiO_2 for the considered temperature range, but mainly at the lowest temperatures (9.8, 14.0, and 6.4 % with the TiO_2, mTiO_2, and Au/mTiO_2 at 573 K, respectively). The selectivity to ethylene is higher with the mTiO_2 because of its higher concentration of acid and strong basic sites. The former sites promote dehydration reactions via E_2 mechanism, whereas the latter ones (related to isolated O^{2-} anions generated by the TiO_2 surface modification) favour dehydrations through the E_{1cB} pathway [55]. Furthermore, selectivity to ethylene (dehydration to olefins) is favoured over the selectivity to diethyl ether (dehydration to ethers) as temperature increases [55].

Regarding to the 1,3-butadiene also obtained in dehydration steps, selectivities with the TiO_2 and mTiO_2 materials are between 2.5 and 5.0 times lower than the 1-butanol selectivities. This fact suggests that these catalysts are as selective to 1-butanol as other materials tested in this reaction (1-butanol/1,3-butadiene ratios of 2.3 and 7.6 at 673 K with magnesia and hydroxyapatites, respectively) [51,56]. However, no butadiene was observed in the studied temperature range when using the Au/mTiO_2 catalyst. This fact corroborates that the use of a bifunctional catalyst, and hydrogen presence, promotes the hydrogenation of the C=C bond. Similar conclusions have been recently reported in the selective hydrogenation of butadiene

using an Au/TiO_2 catalyst [57]. Although temperatures higher than 573 K are needed for yielding significant butanol selectivities with the Au-free materials (3.2 and 2.0 % at 623 K with the TiO_2 and $mTiO_2$, respectively), a significant selectivity is observed with the $Au/mTiO_2$ at 523 K (9.4 %).

The increase on the 1-butanol selectivity observed for the Au-doped catalyst, is not only related with the higher amounts of acetaldehyde formed over this catalyst (specially at the lowest temperatures) but also to the role of the metal in the hydrogen transfer steps leading to the formation of butanol. At the first point, it should be noted that condensation of acetaldehyde is a relatively fast reaction at these conditions [14], but the butanol/acetaldehyde ratios are higher for the $Au/mTiO_2$ catalyst (0.26, 0.06, and 0.37 with TiO_2, $mTiO_2$, and $Au/mTiO_2$ at 673 K, respectively). Concerning to the promoting effect of the gold on hydrogen-transfer effects, it should be noted that low-size supported gold nanoparticles can dissociate chemisorbed H_2 at low temperatures and catalyse hydrogenations at ambient conditions.

In order to gain further understanding on the reaction mechanism, the formation of minor products was analysed, being this information summarized in the **Table 2**. Selectivities to butanal (obtained from crotonaldehyde C=C bond hydrogenation) are always higher for the $Au/mTiO_2$ catalyst (1.6, 0.5, and 2.6 % at 673 K for TiO_2, $mTiO_2$, and $Au/mTiO_2$, respectively), being the highest at 523 K (7.0 %) according to the gold hydrogenation ability at low temperatures. Selectivities to crotyl alcohol (formed by the C=O hydrogenation of crotonaldehyde) are always lower than those obtained to butanal at each temperature (0.1, 0.2, and 0.1 % at 673 K with TiO_2, $mTiO_2$, and $Au/mTiO_2$, respectively). Concerning the butanal/crotyl alcohol ratios, improvements of 57 and 400 % are reached when comparing the $Au/mTiO_2$ catalyst with the TiO_2 and $mTiO_2$, respectively. This enhancement is mainly due to the small Au nanoparticles which essentially promotes the hydrogenation of the C=C bond [6]. Although small gold particles promote the hydrogenation of C=C bonds versus the reduction of

the C=O group, Au/mTiO_2 seems to promote also the crotonaldehyde reduction to 1-butanol. This result suggests that this metal can also promote MPV-type hydrogen transfer reaction. Consequently, gold nanoparticles addition over the titania catalyst surface and hydrogen supplying enhance both alcohol dehydrogenation and C=C double bond hydrogenation steps promoting the production of 1-butanol. These effects are more marked at low temperatures at which dehydrations are not yet favoured.

The analysis of the minor products summarized in **Table 2** reveals that Au/mTiO_2 also provides significant selectivities to higher alcohols (up to 6.6 %), especially at the lowest temperatures. These values decrease as temperature rises due to the increasing importance of dehydration steps at the highest temperatures. Concerning the TiO_2 and mTiO_2, only significant selectivities for the formation of diethyl ether, acetaldehyde, or ethylene were observed below 623 K. Once again, the positive effect of the metal both in terms of enhancing dehydrogenation steps yielding acetaldehyde, and hydrogenating unsaturated C4 moieties justify these effects. In good agreement with this second effect, acetaldehyde selectivities decrease as temperature increases (but below 573 K) for the catalysts without gold. However, the selectivity to acetaldehyde increases again above 573 K, when hydrogen-transfer reactions start to be important, shifting the overall reaction towards the formation of the butanol, intermediates and acetaldehyde. In the case of the Au/mTiO_2 catalyst, the acetaldehyde selectivity decreased from 523 to 623 K, but then it kept almost constant for the two highest temperatures, being only noticed differences between diethyl ether and ethylene selectivities. Concerning to other minor products, smaller amounts of products coming for acetaldehyde oxidation were observed (acetic acid and ethyl acetate) which are presumably formed by Cannizzaro-type and Tishchenko-type mechanisms [55]. It should be noted that the formation of methane was not observed in any case, discarding that the involved active phases participate in C-C cleavage reactions.

Conversions, carbon balances, and selectivities to the main products working under inert conditions with the three materials are shown in **Figure 6**. In the cases of the non Au-loaded catalysts, all the results are almost the same that those obtained with hydrogen supplying. This fact has sense since these materials lack the active metal sites needed to dissociate the hydrogen molecule. On the other hand, the conversions observed with the Au/mTiO_2 material were much lower than the previously obtained in the reaction while hydrogen feeding (drop of 32 % at 673 K), and even lower than those observed at high temperatures with the TiO_2 catalyst. In this case (using the Au-doped catalyst), the absence of hydrogen in the gas phase leads to lower catalytic activity. This fact suggests both, that dehydrogenation of ethanol to acetaldehyde is not an equilibrium-limited step (in this case, the presence of hydrogen will reverse the equilibrium), and that hydrogen transfer effects play a significant role in the overall reaction. This change in the activity of the catalyst implies different product distribution, mainly at the lowest temperature. Thus, the acetaldehyde selectivity at 523 K was 16 % higher than the obtained under reductive conditions. As to the 1-butanol production, no selectivity was observed at the lowest temperature (at which the maximum value was noticed when introducing hydrogen to the reactor). Moreover, the selectivities to crotonaldehyde and crotyl alcohol (crotonaldehyde-to-butanol alkene intermediate) were 3.2 and 1.7 % (increases of 60 and 70 % comparing with the values reached while hydrogen feeding). These results suggest that the hydrogenations are the rate-determining steps when working under inert conditions with the Au/mTiO_2 catalyst at low temperatures. Thus, the hydrogen supplying has a positive effect on the ethanol-to-butanol yield improvement when using this bifunctional catalyst. Besides, the good performance of gold nanoparticle supported materials on selective hydrogenation of the C=C bond is confirmed, since the formation of crotyl alcohol is reduced in a greater extent than crotonaldehyde (hydrogenation of the C=O) when hydrogen is supplied.

Concerning the results obtained at 573 K, the higher acetaldehyde formation directly conditions the selectivity to 1-butanol (2.1 %). At the two highest temperatures, the product

distribution was similar to the obtained with the TiO_2 and $mTiO_2$ catalysts, with the exception of the butanal formation through 1-butanol dehydrogenation because of the metal phase presence (1.9% at 673 K with the $Au/mTiO_2$, whereas it was not produced with the other two materials). Low selectivities to 1,3-butadiene (< 0.8 %) were observed with the $Au/mTiO_2$ whenever 1-butanol was formed. Furthermore, the carbon balances obtained with the Au-doped material were higher than those observed when working with hydrogen feeding (especially at the highest temperature), mainly because of the lower attained conversions (less relevance also of side reactions).

In order to determine the individual role of gold, an inert support was also used to prepare the metal catalyst and its activity was compared at same reaction conditions. In a preliminary test, the activity of SiO_2 supported (without any metal phase) was corroborated by carrying out a blank test at same reaction conditions without observing any ethanol conversion even at the highest temperature. As consequence, this support is chosen to individually analyse the role of the metal phase with assurance of no disturbances. Main results obtained with the Au/SiO_2 catalyst are shown in **Figure 7**. In general terms, ethanol conversions are significantly lower than with the titania-based catalysts. These conversions were higher when working under inert conditions, especially at lower temperatures. This fact suggests a high hydrogenation activity of Au nanoparticles. This process is involved in the elementary step of ethanol to acetaldehyde. When an acid/basic material is introduced in the medium, the aldol condensation of acetaldehyde is fast and displaces the equilibrium between these two compounds. In absence of these sites, the reverse reaction (acetaldehyde hydrogenation to ethanol) prevails over the direct one, implying final lower conversions. Furthermore, the higher differences noticed at lower temperatures indicate that, with the supported gold nanoparticles, dehydrogenation is favoured against hydrogenation as temperature increase. This is in agreement with the high activity shown by these materials in hydrogenation reactions at low temperatures [3]. Carbon balance and selectivity to acetaldehyde are close to 100 % in

each case (for any tested temperature and reaction conditions), confirming the hydrogenation/dehydrogenation role of the gold phase and the negligible activity of this material for other type of reactions promoted by the acid-base component of the catalyst (such as aldol condensations).

3.3 Analysis of used catalysts

Considering that deactivation because of metal sinterization is identified as the main drawback of using Au/TiO_2 to catalyse reactions at severe thermal conditions, the spent catalysts recovered after these reactions were analysed to study the behaviour of $Au/mTiO_2$ and identify any possible improvement respect to the expected one. Electron microscopy analysis of the spent $Au/mTiO_2$ was carried out in order to confirm if there is any relevant change in the gold particles during all the process. A representative microscopy of this analysis, as well as the corresponding histogram, is shown in **Figure 8**. In this figure, the analogous analysis of Au/SiO_2 is also plotted, in order to compare the evolution of gold supported on an inert or active material. Both microscopies correspond to results obtained at inert conditions at 673 K, the worst conditions. The analysis of the other conditions revealed similar conclusions. Despite the relative differences that can be noticed when comparing the particle size distribution of both catalysts with those obtained with the fresh materials (**Fig. 3**), the mean particle sizes (6.0 and 4.9 nm for $Au/mTiO_2$ and Au/SiO_2, respectively) were kept in similar values. Taking into account that sinterization was not observed after reaction at the highest temperature tested, the possibility of changes in the metal dispersion that could strongly condition the experimental results was discarded.

3.3 DRIFT spectroscopy

In order to better understand the activity results, the evolution of adsorbed species on each material was analysed by DRIFT spectroscopy. Spectra of the materials recorded at reaction temperatures in presence of ethanol and under reductive conditions, are included in **Figure 9**. Only wavenumbers lower than 1800 cm^{-1} have been considered, since these are the bands providing information about the adsorbed bands of compounds involved in this reaction. DRIFT spectra of the Au/SiO_2 material did not show any adsorption band different from that observed by ethanol (1060 cm^{-1}), both under inert and reductive conditions. This behaviour was expected since SiO_2 is an inert support and acetaldehyde is weakly adsorbed even on TiO_2. In the case of $mTiO_2$ spectra (**Fig. 9b**), clear absorption bands are observed in the region below 1100 cm^{-1}. Within this region, two adsorption bands are distinguished: the first one, at 940 cm^{-1}, is related to the CO symmetric-stretching vibration mode of the diethyl ether [58]; the second one, at 1060 cm^{-1}, is associated with the CO stretching vibration mode of ethoxy species and CO asymmetric-stretching of diethyl ether [58-59]. These results demonstrate that species adsorbed on the titania surface are mainly ethoxy and diethyl ether, especially at low temperatures, being in agreement with the gas phase results. There is other region above 1200 cm^{-1} in which different absorption bands are observed (1210 and 1390 cm^{-1}), related to acetate species and CH_3 bending vibration mode of mainly ethoxides, respectively [20,59]. Nevertheless, the intensity of these adsorption bands are almost negligible regarding to those mentioned above in the first region.

Concerning the parent TiO_2 material (**Fig. 9a**), it can be assessed the same characteristic adsorption bands as the $mTiO_2$ catalyst. However, their identification is more difficult than with the $mTiO_2$ because the bands (especially 940 and 1060 cm^{-1}) are weaker. Furthermore, the intensities of the different bands change as temperature rises without following a uniform trend, whereas they continuously decrease when the $mTiO_2$ is used. In the non-modified catalyst, the decrease in the spectrum intensity from 523 to 573 K is due to temperature

increase, because desorption is and endothermic process and the compounds produced in the reaction are the same as those obtained at 523 K. However, above 573 K, the conversion significantly increases as temperature rises, and 1-butanol and higher alcohols (selectivities of 5.0 and 1.2 % at 673 K, respectively) obtained are strongly adsorbed on the TiO_2. Consequently, the intensity of the spectra increases at the highest temperatures. This fact does not occurs with the $mTiO_2$ since 1-butanol and higher alcohols are not obtained in such a larger extent (selectivities of 1.9 and 0.1 % at 673 K, respectively) leading to a decrease of the band intensities as temperature rises. In general terms, the intensity of the spectra is higher with the $mTiO_2$ material than with the TiO_2 (except at the highest temperature because of the heavy compound adsorption). This fact is due to the higher surface concentration of active sites on the $mTiO_2$ catalyst, which promotes the stabilization of the starting ethanol and the reaction products.

Regarding to the Au/$mTiO_2$ catalyst (**Fig. 10c**), the intensity of the absorption bands at each temperature is lower than the observed with the other materials because of its lower concentration of active sites and the metal phase presence. However, at the two lowest temperatures, it can be noticed that the relative significance of the band associated to the CO symmetric-stretching vibration mode of diethyl ether (940 cm^{-1}) is much lower than other bands, in comparison with the TiO_2 and $mTiO_2$ catalysts. This is in agreement with the lower amounts of diethyl ether observed in the gas phase when this catalyst is used at these conditions (**Fig. 6c**). Therefore, the band appearing at 1060 cm^{-1}, associated with the CO stretching vibration mode of ethoxides as diethyl ether, is almost negligible with this material. A new band at 870 cm^{-1} related to the CH_3 rocking vibration mode of acetaldehyde [58] is observed at low temperatures, and it is still observed even at rising temperatures. This band, as well as band at 1710 cm^{-1} (C=O stretching vibration mode of acetaldehyde), confirm the presence of acetaldehyde over the catalytic surface [59], endorsing the high ability of this material to dehydrogenate ethanol because of the active metal. At the highest temperature ,

different bands related to molecules strongly adsorbed on the catalyst surface are observed. Bands at 1430 cm^{-1} start to appear at 623 K, being associated with strongly adsorbed acetate species [20]. Other two bands at 730 and 1165 cm^{-1} begin to be significant at the same temperature, being the former related to the CH_2 bending vibration mode of molecules with more than four CH_2 groups [60], and the latter associated with the C-C stretching mode [59]. These results corroborate the production of heavier molecules at the highest temperatures, which remain strongly adsorbed on the surface. The rise of the band at 1660-1740 cm^{-1} (C=O stretching vibration mode of aldehydes), suggests that these strongly adsorbed species are mainly higher aldehydes produce by subsequent aldol condensations in agreement with the high activity of this material especially at the highest temperatures.

Spectra recorded when working under inert conditions were similar for both TiO_2 and $mTiO_2$ materials, whereas differences were observed with the Au/$mTiO_2$ catalyst. This is in agreement with the results previously observed by the gas phase analyses. **Figure 10** shows the spectra collected for the Au/$mTiO_2$ when working at inert conditions. The lower catalytic activity and hydrogenation ability justify the differences with results at reductive conditions. Thus, the bands associated with the long chain molecules either disappeared (730 cm^{-1}), or were markedly reduced (1165 cm^{-1}). Furthermore, a new low-intensity band (1590 cm^{-1}) corresponding to the stretching vibration mode of the C=C bond arose as temperature increased [45]. This fact together with the rise of the relative significance of the band associated with the C=O stretching vibration mode (1740 cm^{-1}) and the no formation of higher aldehydes and alcohols indicates that mainly crotonaldehyde and crotyl alcohol were adsorbed on the Au/$mTiO_2$ catalyst when working under inert conditions.

A global analyses of all these results suggests that working with a bifunctional catalyst and with hydrogen supplying not only allows improving the C4 obtaining, but also the stability of the catalyst since the product adsorption on the catalytic surface is reduced, preventing the deactivation of the acid-base component of the catalyst. This hypothesis is agreement with a

work recently performed by Wang and co-workers dealing with similar C-C bond formation reactions [61].

4. CONCLUSIONS

A relevant improvement in the ethanol gas phase condensation is observed when reaction is catalysed by gold nanoparticles supported on TiO_2. The commercial P25 is modified by including extra Ti(IV) cations, resulting into a very disperse and thermal stable material. Experimental results demonstrate an increase in the ethanol conversion (up to 74.2 %), butanol selectivity (8.3 %) and a considerable decrease in the intramolecular and intermolecular ethanol dehydration (no butadiene observed with $Au/mTiO_2$), reactions directly related to undesired products. The presence of these nanoparticles plays a key role in intermediate steps, enhancing the formation of acetaldehyde by dehydrogenation and the hydrogenation of C4 unsaturated molecules. These positive effects are more marked in presence of molecular hydrogen, whereas the presence of this gas has not any noticeable effect on the performance of the other titania based catalysts studied in this work.

DRIFT spectra explain the activity results, showing the high decrease of the ethoxides adsorbed over the catalytic surface when the gold nanoparticles are present over titania. Accordingly, the undesirable strong adsorption of ethanol on titania is reduced by using bifunctional materials. This strategy also allows working at softer conditions at which the competitive side reactions (dehydrations) are not favoured.

Acknowledgements

The authors thank financial support from the Ministry of Economy and Competitiveness of the Spanish Government (Contract CTQ2014-52956-C3-1-R). J. Quesada would also like to acknowledge the local Government of the Principality of Asturias (Spain) for his Ph.D.

fellowship of the Severo Ochoa Program (PA-14-PF-BP14-105). R. Arreola-Sánchez thanks the CONACYT (Mexico) for the mobility grant (291212) for Ph.D. stay at the University of Oviedo.

References

1. A. Corma, H. García, Chem. Soc. Rev. 37 (2008) 2096-2126.
2. A.S.K. Hashmi, Chem. Rev. 107 (2007) 3180-3211.
3. M. Haruta, Chem. Rec. 3 (2003) 75-87.
4. G.C. Bond, P.A. Sermon, G. Webb, D.A. Buchanan, P.B. Wells, J. Chem. Soc. Chem. Commun. (1973) 444-445.
5. A.S.K. Hashmi, G.J. Hutchings, Angew. Chem. Int. Ed. 45 (2006) 7896-7936.
6. P. Claus, A. Brückner, C. Mohr, H. Hofmeister, J. Am. Chem. Soc. 122 (2000) 11430-11439.
7. J.E. Bailie, G.J. Hutchings, Chem. Commun. (1999), 2151-2152.
8. E.V. Makshina, M. Dusselier, W. Janssens, J. Degrève, P.A. Jacobs, B.F. Sels, Chem. Soc. Rev. 43 (2014) 7917-7953.
9. T.J. Schwartz, B.H. Shanks, J.A. Dumesic, Curr. Opin. Biotechnol. 38 (2016) 54-62.
10. L. Tao, J.N. Markham, Z. Hag, M.J. Biddy, Green Chem. 19 (2017) 1082-1101.
11. H. Aitchison, R.L. Wingad, D.F. Wass, ACS Catal. 6 (2016) 7125-7132.
12. J. Sun, Y. Wang, ACS Catal. 4 (2014) 1078-1090.
13. C. Angelici, B.M. Weckhuysen, P.C.A. Bruijnincx, ChemSusChem, 6 (2013) 1595-1614.
14. J.T. Kozlowski, R.J. Davis, ACS Catal. 3 (2013) 1588-1600.
15. S. Hanspal, Z.D. Young, H. Shou, R.J. Davis, ACS Catal. 5 (2015) 1737-1746.
16. C.R. Ho, S. Shylesh, A.T. Bell, ACS Catal. 6 (2016) 939-948.
17. T. Moteki, D.W. Flaherty, ACS Catal. 6 (2016) 4170-4183.
18. S. Link, M.A. El-Sayed, J. Phys. Chem. B, 103 (1999) 8410-8426.
19. J.E. Rekoske, M.A. Barteau, Ind. Eng. Chem. Res. 50 (2011) 41-51.
20. Z.D. Young, S. Hanspal, R.J. Davis, ACS Catal. 6 (2016) 3193-3202.
21. H. Yoshitake, Y. Aoki, S. Hemmi, Micropor. Mesopor. Mat. 93 (2006) 294-303.

22. V.L. Sushkevich, I.I. Ivanova, V.V. Ordomsky, E. Taarning, ChemSusChem 7 (2014) 2527-2536.
23. A.M. Nadeem, G.I.N. Waterhouse, H. Idriss, Catal. Today 182 (2012) 16-24.
24. O.A. Simakova, V.I. Sobolev, K.Y. Koltunov, B. Campo, A.R. Leino, K. Kordás, D.Y. Murzin, ChemCatChem 2 (2010) 1535-1538.
25. R. Zanella, C. Louis, Catal. Today 107-108 (2005) 768-777.
26. V.I. Sobolev, K.Yu. Koltunov, O.A. Simakova, A. Leino, D.Yu. Murzin, Appl. Catal. A 433-434 (2012) 88-95.
27. N. Hammer, I. Kvande, D. Chen, M. Ronning, Catal. Today 122 (2007) 365-369.
28. D. Boyd, S. Golunski, G.R. Hearne, T. Magadzu, K. Mallick, M.C. Raphulu, A. Venugopal, M.S. Scurrel, Appl. Catal. A 292 (2005) 76-81.
29. M. Haruta, Gold Bulletin 37 (2004) 27-36.
30. F. Buccuzzi, A. Chiorino, M. Manzoli, P. Lu, T. Akita, S. Ichikawa, M. Haruta, J. Catal. 202 (2001) 256-267.
31. G.M. Veith, A. R. Lupini, S. Rashkeev, S.J. Pennycook, D.R. Mullins, V. Schwartz, C.A. Bridges, N.J. Dudney, J. Catal. 262 (2009) 92-101.
32. C. Wang, H. Wang, Q. Yao, J. Li, J. Lu, J. Phys. Chem. C 120 (2016) 478-486.
33. R. Meyer, C. Lemire, Sh.K. Shaikhutdinov, H.J. Freund, Gold Bulletin 37 (2004) 72-114.
34. R. Zanella, L. Delannoy, C. Louis, Appl. Catal. A 291 (2005) 62-72.
35. R. Zanella, S. Giorgio, C. R. Henry, C. Louis, J. Phys. Chem. B 106 (2002) 7634-7642.
36. M. Azar, V. Caps, F. Morfin, J.L. Rousset, A. Piednoir, J.C. Bertolini, L. Piccolo, J. Catal. 239 (2006) 307-312.
37. L. Stradella, M. Argentero, Thermochimica Acta 219 (1993) 315-323.
38. G.C. Bond, C. Louis, D.T. Thompson, in: G. J. Hutchings (Eds.), Catalysis by Gold, London, 2006, Vol. 6, p. 111.
39. A. Hugon, N.E. Kolli, C. Louis, J. Catal. 274 (2010) 239-250.

40. R. Zanella, S. Giorgio, C.H. Shin, C.R. Henry, C. Louis, J. Catal. 222 (2004) 357-367.

41. M. León, E. Díaz, S. Bennici, A. Vega, S. Ordóñez, A. Auroux, Ind. Eng. Chem. Res. 49 (2010) 3663-3671.

42. F. Arena, R. Dario, A. Parmaliana, Appl. Catal. A 170 (1998) 127-137.

43. R. A. Spurr, H. Myers, Anal. Chem. 29 (1957) 760-762.

44. H. Arnold, F. Döbert, J. Gaube. Handbook of heterogeneous catalysis, 2nd ed., Willey-VCH: Wimheim, 2008; vol 2, p. 740.

45. J. Quesada, L. Faba, E. Díaz, S. Ordóñez, Appl. Catal. A 542 (2017) 271-281.

46. S. Carretin, Y. Hao, V. Aguilar-Guerrero, B.C. Gates, S. Trasobares, J.J. Calvino, A. Corma, Chem. Eur. J. 13 (2007) 7771-7779.

47. M.A. Nadeem, I. Majeed, G.I.N. Waterhouse, H. Idriss, Catal. Struct. React. (2015) 61-70.

48. Y. Guan, E.J. M. Hensen, Appl. Catal. A 361 (2009) 49-56.

49. S. Naya, A. Inoue, H. Tada, ChemPhysChem, 12 (2011) 2719-2723.

50. N. Rahimi, R.A. Pax, E.M. Gray, Prog. Solid State Chem. 44 (2016) 86-105.

51. T. Tsuchida, S. Sakuma, T. Takeguchi, W. Ueda, Ind. Eng. Chem. Res. 45 (2006) 8634-8642.

52. J.T. Kozlowski, R.J. Davis, J. Energy Chem. 22 (2013) 58-64.

53. S. Ordóñez, E. Díaz, M. León, L. Faba, Catal. Today 167 (2011) 71-76.

54. T. Tsuchida, J. Kubo, T. Toshioka, S. Sakuma, T. Takeguchi, W. Ueda, J. Catal. 259 (2008) 183-189.

55. J.I. Di Cosimo, C.R. Apesteguía, M.J.L. Ginés, E. Iglesia, J. Catal. 190 (2000) 261-275.

56. A. Chieregato, J.V. Ochoa, C. Bandinelli, G. Fornasari, F. Cavani, M. Mella, ChemSusChem 8 (2015) 377-388.

57. N. Masoud, L. Delannoy, H.L. Schaink, A.M.J. van der Eerden, J.W. de Rijk, T.A.G. Silva, D. Banerjee, J.D. Meeldijk, K.P. de Jong, C. Louis, P.E. de Jongh, ACS Catal. 7 (2017) 5594-5603.

58. T. Shimaouchi, In Tables of Molecular Vibrational Frequencies Consolidated Volumes, U.S. National Bureau of Standards (NSRDS-NBS 39), 1972; Vol. 1, pp.1-160.

59. J.E. Rekoske, M. A. Barteau, Langmuir 15 (1999) 2061-2070.

60. B.C. Smith, in: CRC Press LLC (Eds.), Infrared Spectral Interpretation: A systematic Approach, CRC Press LLC: Florida, 1998, p.36.

61. S. Wang, K. Goulas, E. Iglesia, J. Catal. 340 (2016) 302-320.

SCHEME CAPTION

Scheme 1. Proposed ethanol condensation pathway by the four-step mechanism. Symbols: (A) ethanol; (B) acetaldehyde; (C) crotonaldehyde; (D) crotyl alcohol; (E) butanal; (F) 1-butanol; (G) 1,3-butadiene; (H) ethylene; (I) diethyl ether; (J) ethyl acetate.

FIGURE CAPTION

Figure 1. Characterization of basicity and acidity: (a) CO2-TPD; (b) NH_3-TPD. Symbols: P25 (continuous line); mP25 (long dashes); AumP25 (dotted line).

Figure 2. XRD diffractograms of a) TiO_2, b) $mTiO_2$, and c) $Au/mTiO_2$. Corresponding peak's crystalline phase: A, anatase; R, rutile; Au, gold; planes in brackets.

Figure 3. STEM-HAADF image of the (a) $Au/mTiO_2$ and (b) Au/SiO_2 materials. Analysis of gold particle size distribution.

Figure 4. Diffuse-reflectance UV-Vis spectra of the $Au/mTiO_2$ catalyst (dashed lines: deconvolution of the gold SPR absorption band).

Figure 5. Conversion, carbon balance, and selectivity evolution in the gas phase ethanol condensation under reducing conditions over: a) TiO_2, b) $mTiO_2$, and c) $Au/mTiO_2$. (WHSV = 7.9 h^{-1}; He-H_2 flow). Symbols: conversion (●), carbon balance (▲). Bars: acetaldehyde (yellow), ethylene (blue), diethyl ether (purple), 1-butanol (red), 1,3-butadiene (green), and others (grey).

Figure 6. Conversion, carbon balance, and selectivity evolution in the gas phase ethanol condensation under inert conditions over: a) TiO_2, b) $mTiO_2$, and c) $Au/mTiO_2$. (WHSV = 7.9 h^{-1}; He flow). Symbols: conversion (●), carbon balance (▲). Bars: acetaldehyde (yellow), ethylene (blue), diethyl ether (purple), 1-butanol (red), 1,3-butadiene (green), and others (grey).

Figure 7. Conversion (●), carbon balance (▲), and acetaldehyde selectivity (■) evolution in the gas phase ethanol condensation over Au/SiO_2 under: a) reductive conditions ($He-H_2$ flow), and b) inert conditions (He flow). (WHSV = 7.9 h^{-1}).

Figure 8. STEM-HAADF images and gold nanoparticle distributions of the spent catalysts recovered after 8 hours of reaction under inert conditions at 673 K: a) $Au/mTiO_2$, and b) Au/SiO_2.

Figure 9. DRIFT spectra in the gas phase ethanol condensation under reductive conditions over: a) TiO_2, b) $mTiO_2$, and c) $Au/mTiO_2$.

Figure 10. DRIFT spectra in the gas phase ethanol condensation over $Au/mTiO_2$ under inert conditions

TABLE CAPTION

Table 1. Main results of the fresh catalysts characterization: morphological properties, and density and distribution of the acid and basic sites.

Table 2. Selectivities to side compounds produced with the different catalysts in the gas-phase ethanol condensation. (WHSV = 7.9 h^{-1}; $He-H_2$ flow, 10 vol % H_2).

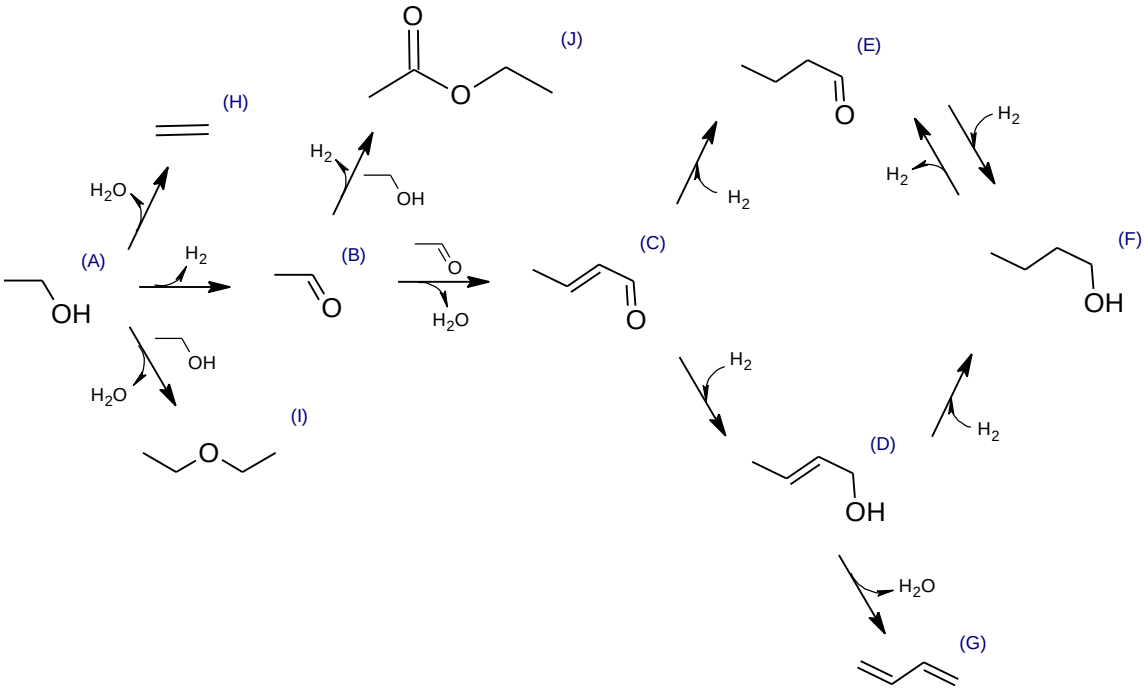

Scheme 1

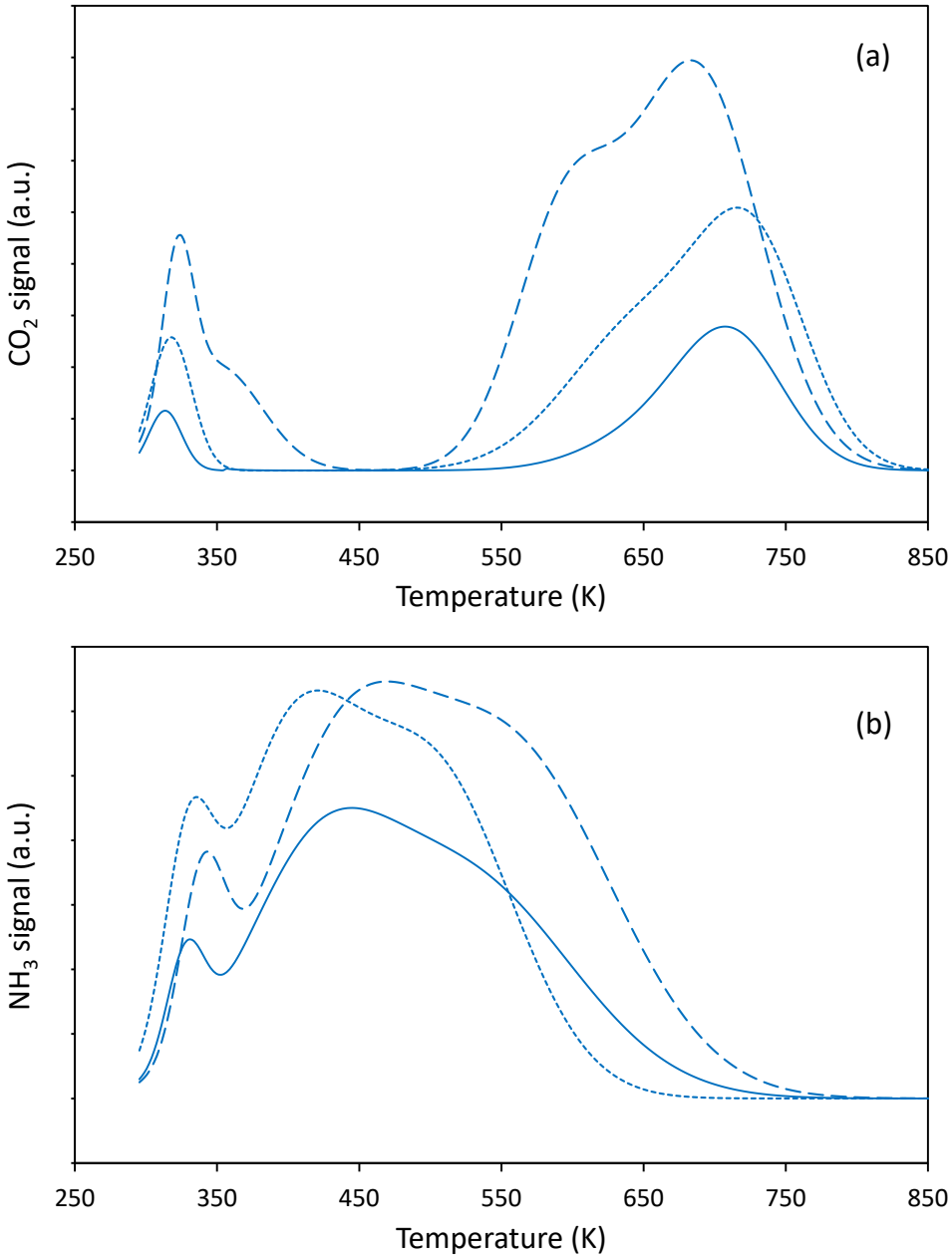
(a)
CO_2 signal (a.u.)
250
350
450
550
650
750
850
Temperature (K)
(b)
NH_3 signal (a.u.)
250
350
450
550
650
750
850
Temperature (K)

Figure 1

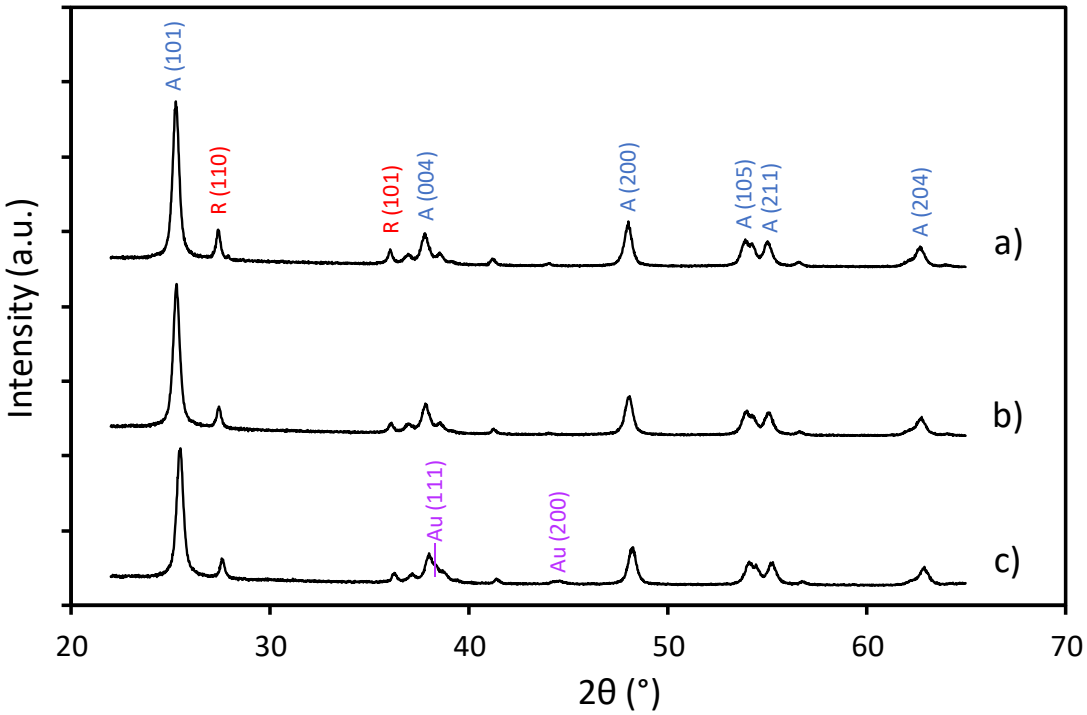
A (101)
R (110)
R (101)
A (004)
A (200)
A (105)
A (211)
A (204)
a)
b)
Au (111)
Au (200)
c)
Intensity (a.u.)
20
30
40
50
60
70
2θ (°)

Figure 2

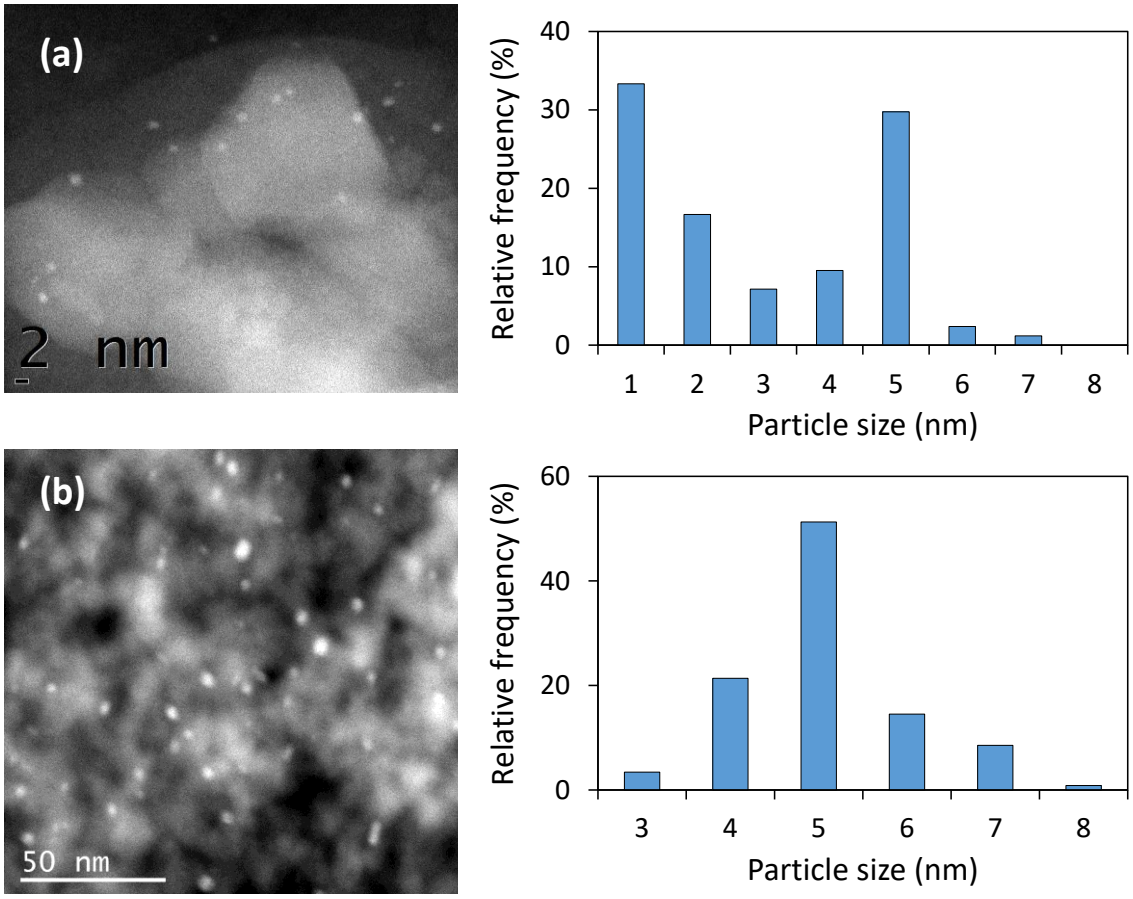
(a)
2 nm
Relative frequency (%)
40
30
20
10
0
1
2
3
4
5
6
7
8
Particle size (nm)
(b)
50 nm
Relative frequency (%)
60
40
20
0
3
4
5
6
7
8
Particle size (nm)

Figure 3

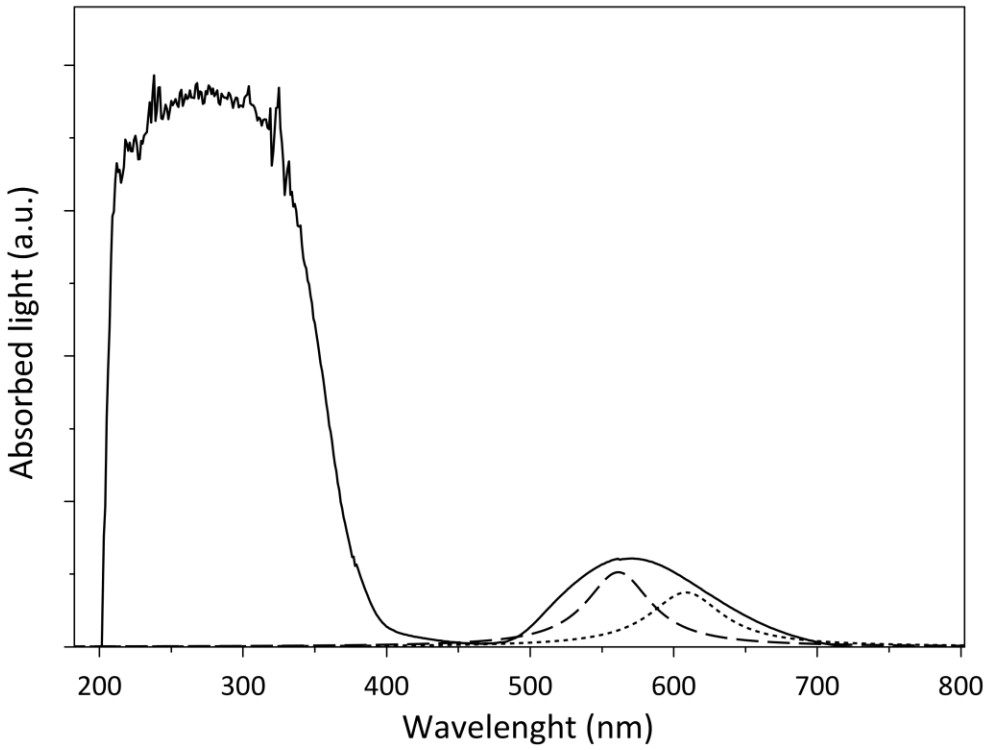

Figure 4

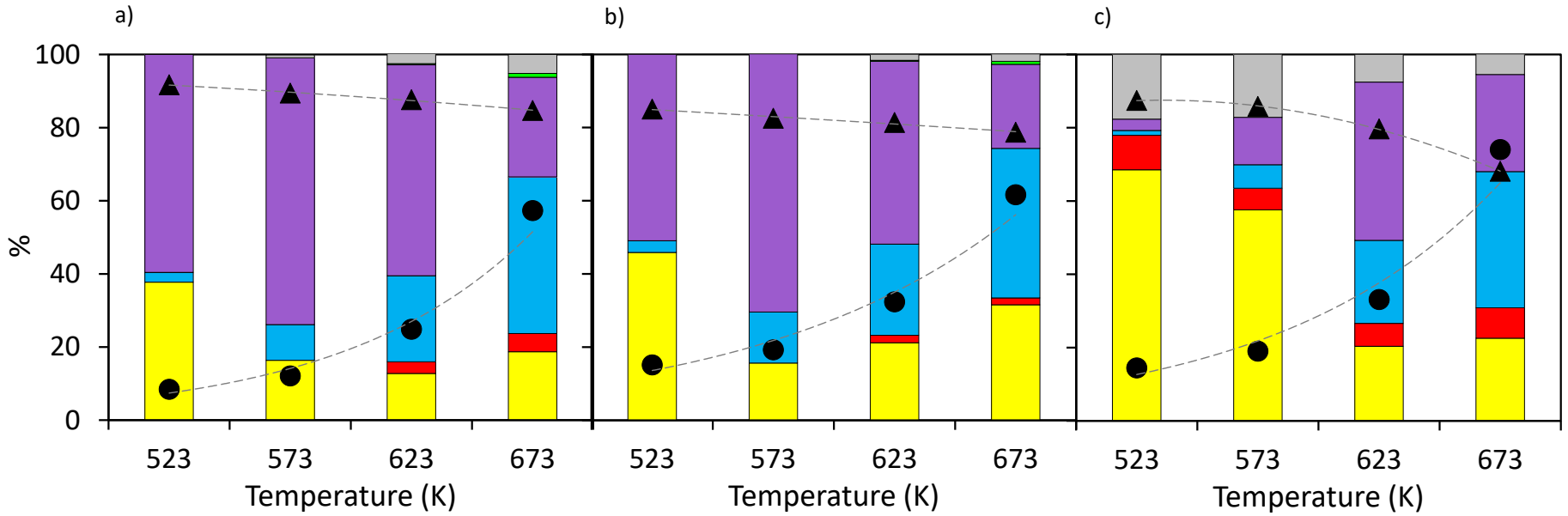

Figure 5

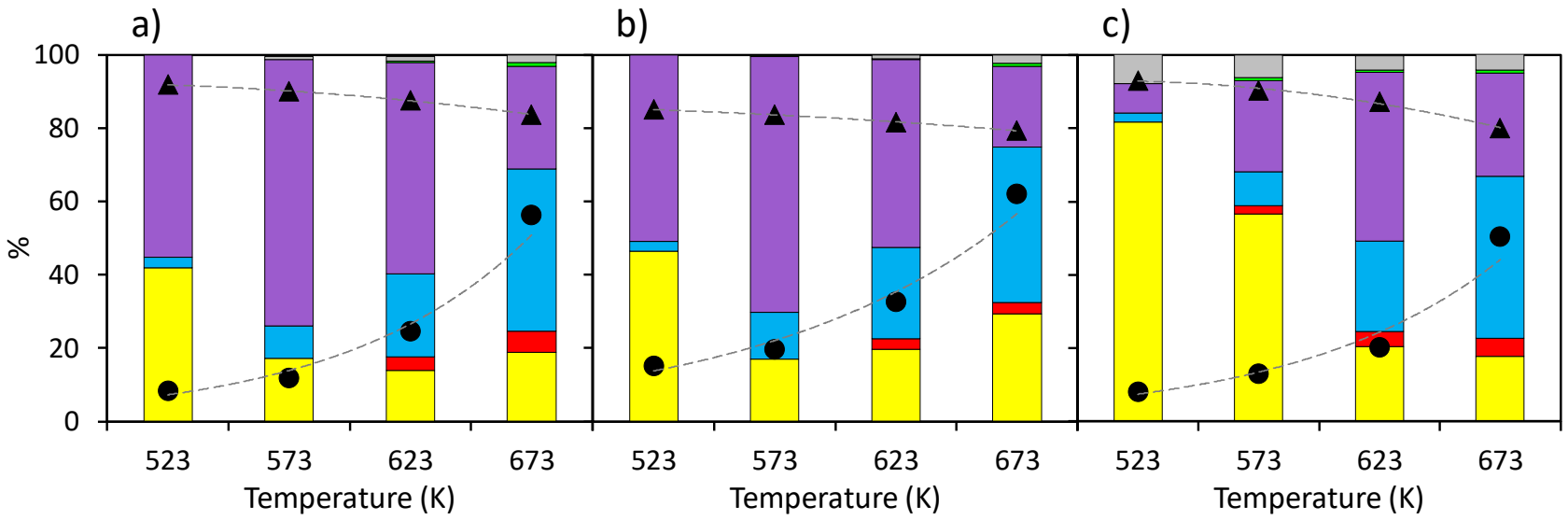

Figure 6

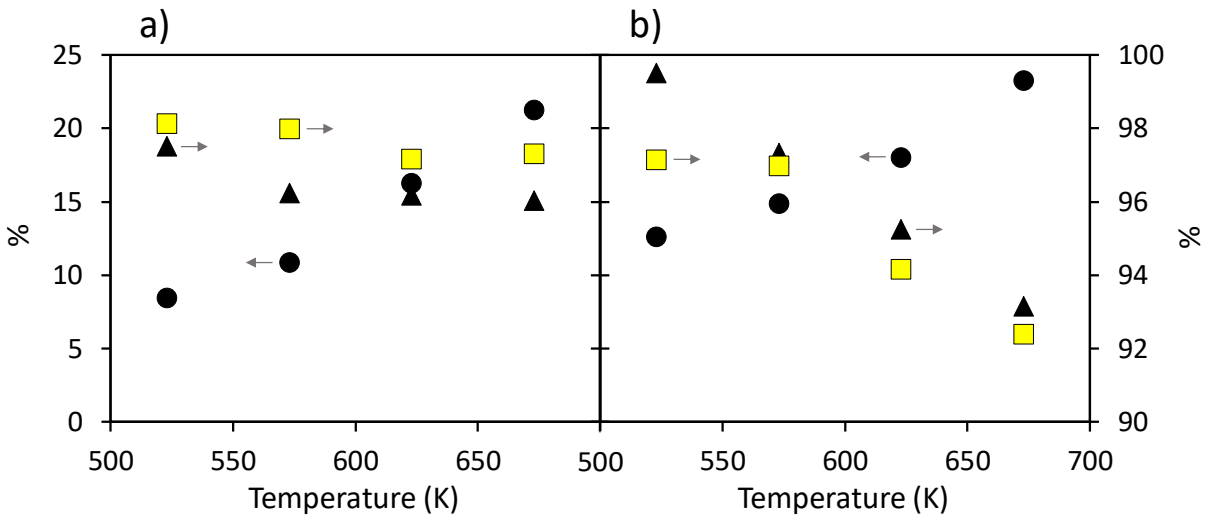
a)
b)
25
20
15
10
5
0
%
100
98
96
94
92
90
%
500
550
600
650
700
Temperature (K)
Temperature (K)

Figure 7

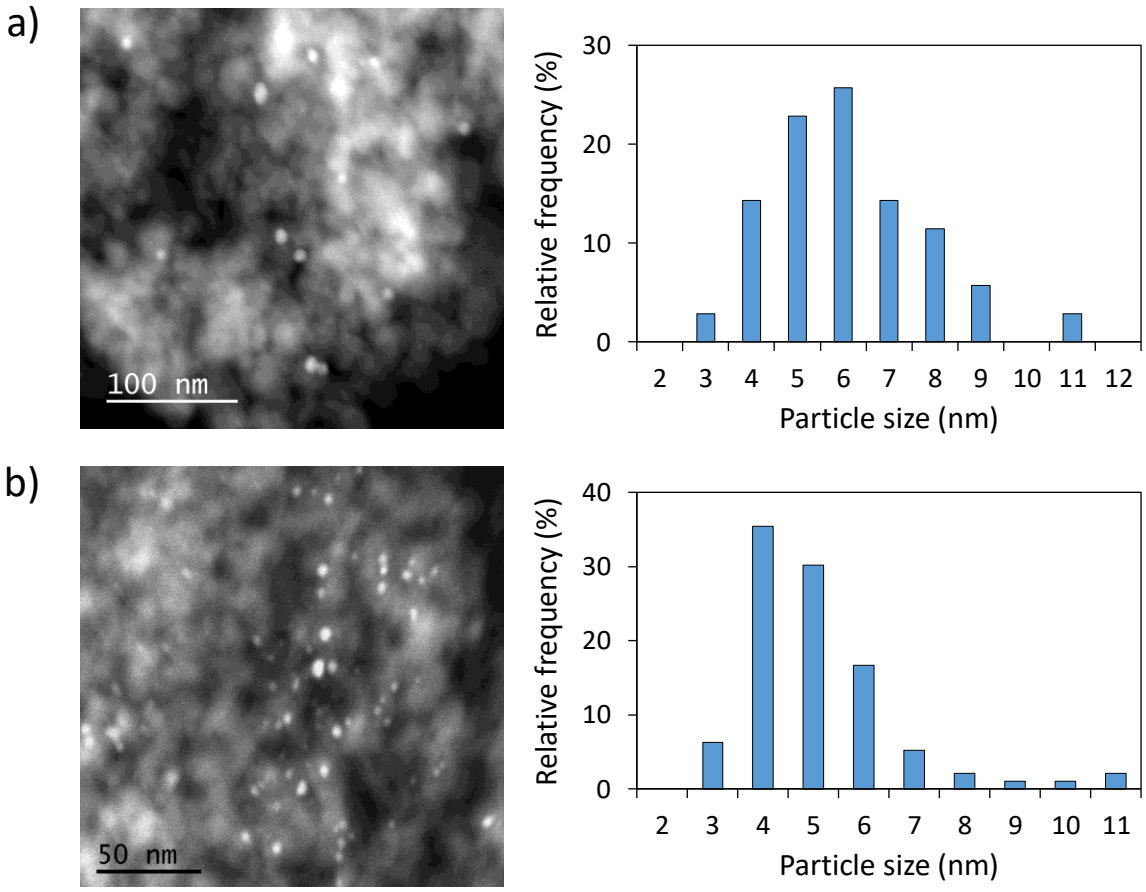
a)
100 nm
Relative frequency (%)
30
20
10
0
2 3 4 5 6 7 8 9 10 11 12
Particle size (nm)
b)
50 nm
Relative frequency (%)
40
30
20
10
0
2 3 4 5 6 7 8 9 10 11
Particle size (nm)

Figure 8

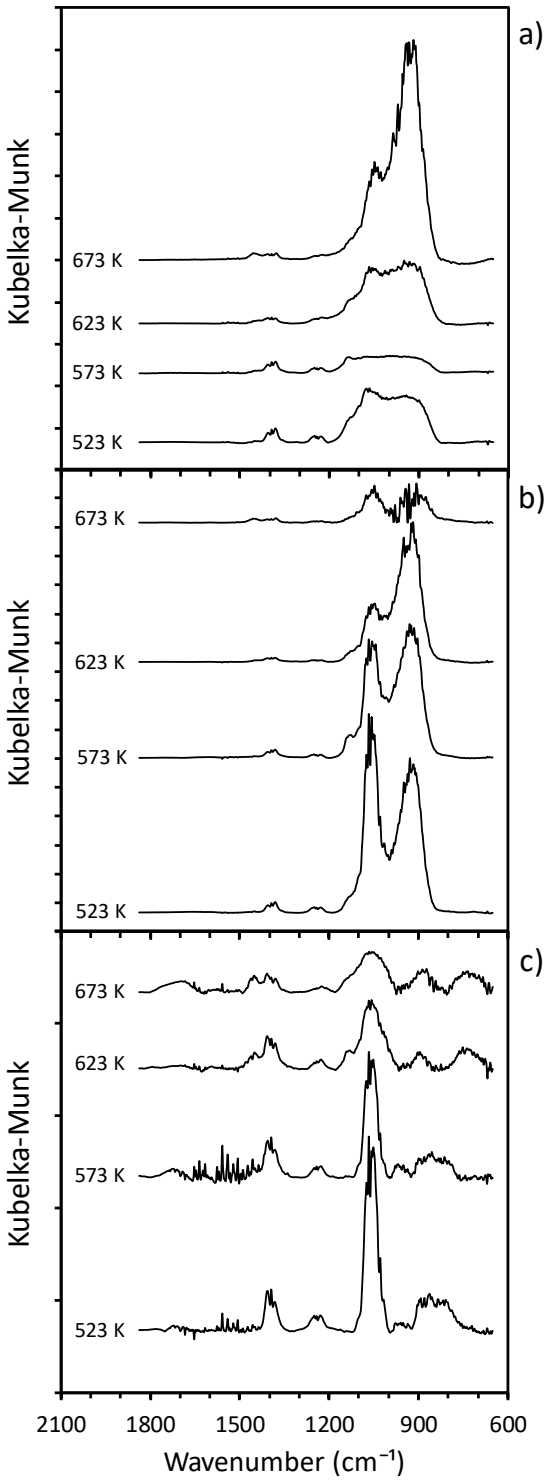
a)
b)
c)
Kubelka-Munk
673 K
623 K
573 K
523 K
2100
1800
1500
1200
900
600
Wavenumber (cm⁻¹)

Figure 9

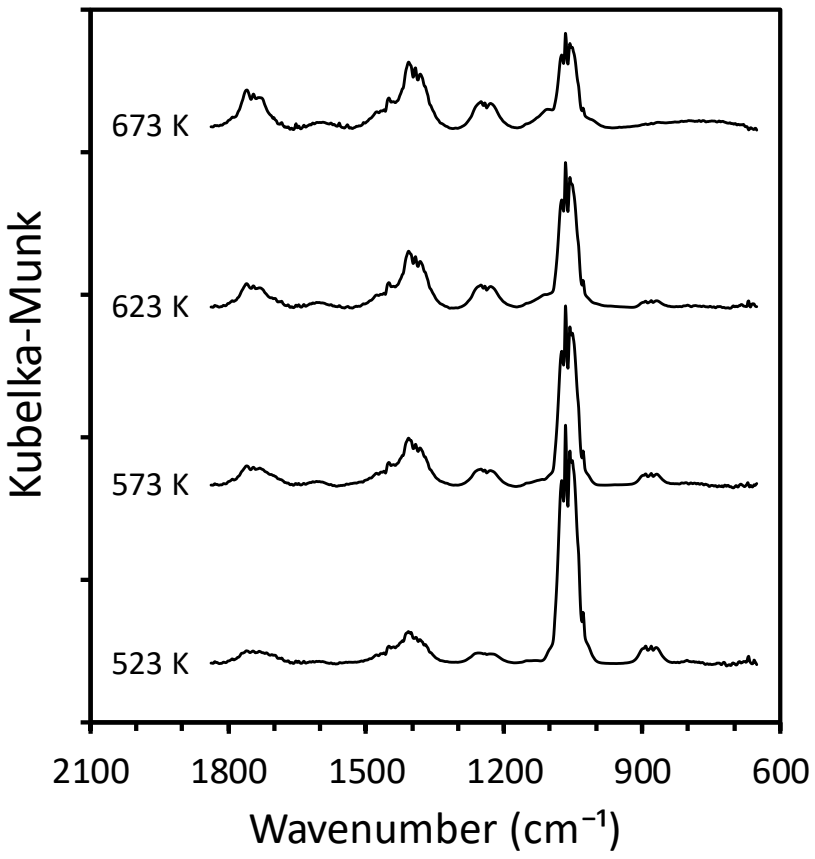
673 K
623 K
573 K
523 K
Kubelka-Munk
2100
1800
1500
1200
900
600
Wavenumber (cm⁻¹)

Figure 10

Table 1. Main results of the fresh catalysts characterization: morphological properties, and density and distribution of the acid and basic sites.

Catalyst	Morphological properties			Acid sites (μmol·g^{-1}), [T (K)]			Basic sites (μmol·g^{-1}), [T (K)]	
	S (m^2·g^{-1})	D_p (nm)	V_p (cm^3·g^{-1})	Weak	Medium	Strong	Weak	Strong
TiO_2	48	19	0.3	0.4 [328]	3.0 [416]	5.1 [523]	2.9 [318]	24.4 [653, 728]
mTiO_2	72	24	0.5	0.8 [340]	5.1 [434]	7.8 [555]	7.7 [322, 350]	42.3 [595, 687]
Au/mTiO_2	49	21	0.3	0.9 [329]	4.7 [400]	5.5 [502]	2.0 [291]	9.9 [664, 714]

Table 2. Selectivities to side compounds produced with the different catalysts in the gas-phase ethanol condensation. (WHSV = 7.9 h^{-1}; He-H_2 flow, 10 vol % H_2).

Catalyst	T (K)	Selectivity (%)								
		Acetic acid	Ethyl acetate	Butanal	Crotonal-dehyde	Crotyl alcohol	2-ethyl-butanol	1-hexanol	2-ethylhexanol	1-octanol
TiO_2	523	0	0	0	0	0	0	0	0	0
	573	0	0	0	0.3	0.5	0	0	0	0
	623	0.4	0.7	0.7	0.5	0.1	0.3	0.2	0.1	0.1
	673	0.8	0.9	1.6	0.2	0.1	0.5	0.5	0.1	0.1
$mTiO_2$	523	0	0	0	0	0	0	0	0	0
	573	0	0	0	0	0	0	0	0	0
	623	0.4	0.5	0.2	0.3	0.1	0.1	0	0	0
	673	0.6	0.8	0.5	0.2	0.2	0.1	0	0	0
$Au/mTiO_2$	523	0	0.8	7.0	2.0	1.0	2.9	3.0	0.5	0.2
	573	1.3	1.6	4.2	5.9	0.8	0.9	0.8	0.8	0.8
	623	0.8	2.1	1.7	1.0	0.2	0.8	0.5	0.3	0.2
	673	0.6	1.2	2.6	0.4	0.1	0.6	0.8	0.1	0.1